Article

Cell Reports

Post-transcriptional Stabilization of *Ucp1* mRNA Protects Mice from Diet-Induced Obesity

Graphical Abstract

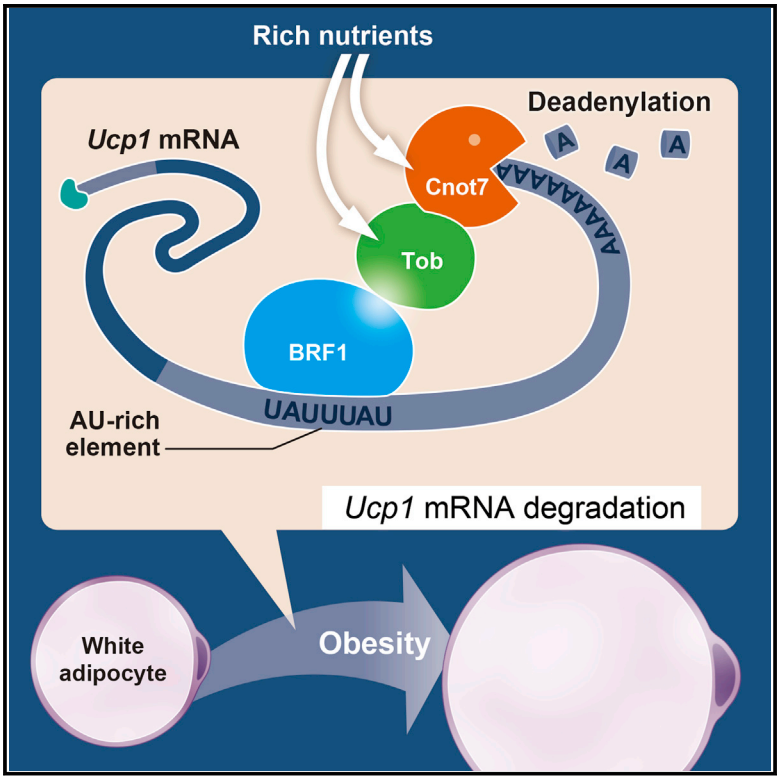

Authors

Akinori Takahashi, Shungo Adachi, Masahiro Morita, Miho Tokumasu, Tohru Natsume, Toru Suzuki, Tadashi Yamamoto

Correspondence

tadashi.yamamoto@oist.jp

In Brief

Takahashi et al. show that the BRF1-Tob-Cnot7 axis exacerbates obesity by post-transcriptionally suppressing *Ucp1* mRNA in iWAT of obese mice. BRF1, which recognizes AU-rich elements, binds to the *Ucp1* 3′-UTR and interacts with Tob. Tob recruits Cnot7 to deadenylate the *Ucp1* mRNA poly(A) tail, resulting in *Ucp1* mRNA degradation.

Highlights

- *Cnot7* and/or *Tob* deficiencies make mice resistant to diet-induced obesity
- Expression of *Cnot7* and *Tob* is augmented in obese iWAT and inhibits Ucp1 level
- Tob interacts with BRF1 at the AU-rich region in the 3′-UTR of *Ucp1* mRNA
- Tob-BRF1 interaction recruits Cnot7 deadenylase to *Ucp1* mRNA for its destabilization

Takahashi et al., 2015, Cell Reports *13*, 2756–2767
December 29, 2015
http://dx.doi.org/10.1016/j.celrep.2015.11.056

CellPress

OPEN ACCESS
CellPress

Cell Reports
Article

Post-transcriptional Stabilization of *Ucp1* mRNA Protects Mice from Diet-Induced Obesity

Akinori Takahashi,[1] Shungo Adachi,[2] Masahiro Morita,[3] Miho Tokumasu,[1] Tohru Natsume,[2] Toru Suzuki,[1] and Tadashi Yamamoto[1,*]

[1]Cell Signal Unit, Okinawa Institute of Science and Technology, Kunigami, Okinawa 904-0412, Japan
[2]Molecular Profiling Research Center for Drug Discovery, National Institute of Advanced Industrial Science and Technology, Tokyo 135-0064, Japan
[3]Department of Biochemistry and Goodman Cancer Research Centre, McGill University, Montréal, QC H3A 1A3, Canada
*Correspondence: tadashi.yamamoto@oist.jp
http://dx.doi.org/10.1016/j.celrep.2015.11.056

SUMMARY

Uncoupling protein 1 (Ucp1) contributes to thermogenesis, and its expression is regulated at the transcriptional level. Here, we show that Ucp1 expression is also regulated post-transcriptionally. In inguinal white adipose tissue (iWAT) of mice fed a high-fat diet (HFD), Ucp1 level decreases concomitantly with increases in Cnot7 and its interacting partner Tob. HFD-fed mice lacking *Cnot7* and *Tob* express elevated levels of *Ucp1* mRNA in iWAT and are resistant to diet-induced obesity. *Ucp1* mRNA has an elongated poly(A) tail and persists in iWAT of *Cnot7*$^{-/-}$ and/or *Tob*$^{-/-}$ mice on a HFD. *Ucp1* 3′-UTR-containing mRNA is more stable in cells expressing mutant Tob that is unable to bind Cnot7 than in WT Tob-expressing cells. Tob interacts with BRF1, which binds to an AU-rich element in the *Ucp1* 3′-UTR. *BRF1* knockdown partially restores the stability of *Ucp1* 3′-UTR-containing mRNA. Thus, the Cnot7-Tob-BRF1 axis inhibits Ucp1 expression and contributes to obesity.

INTRODUCTION

Obesity and related metabolic diseases increase the risk of diabetes, hypertension, cardiovascular diseases, and cancer. In mammals, fats accumulate in white and brown adipose tissues. White adipose tissue (WAT) stores energy in the form of triglycerides. Brown adipose tissue (BAT) dissipates stored energy as heat; thus, BAT increases energy expenditure and resistance to obesity (Harms and Seale, 2013). Uncoupling protein 1 (Ucp1) is uniquely expressed in BAT mitochondria, where it uncouples respiration to produce heat (Rousset et al., 2004; Ricquier, 2011). Ucp1 activity opposes obesity, whereas Ucp1-ablation in mice impairs thermogenesis and induces obesity (Feldmann et al., 2009). Recently, Ucp1-positive adipocytes have been also identified in white adipose deposits and like those in BAT, also dissipate stored energy (Wu et al., 2013). Thermogenic programs in subcutaneous WAT that include high expression of Ucp1 protect mice from obesity (Kopecký et al., 1995, 1996; Seale et al., 2011). Identification of regulators of Ucp1 expression will facilitate development of therapeutic approaches for treatment of obesity-related diseases.

Precise regulation of gene expression is required for body homeostasis, and dysregulation of gene expression leads to various disorders, including metabolic diseases, immunological diseases, and cancer. Recently, not only transcriptional regulation, but also post-transcriptional mechanisms, including capping, splicing, and degrading of mRNAs, have attracted a great deal of attention for regulation of gene expression. Deadenylase-mediated shortening and removal of poly(A) tails at 3′-ends of eukaryotic mRNAs suppress translation and accelerate mRNA decay (Garneau et al., 2007). The major deadenylase in mammals is the CCR4-NOT complex, which comprises at least ten subunits, Cnot1-Cnot3, Cnot6, Cnot6L, and Cnot7-Cnot11 (Albert et al., 2000; Collart and Timmers, 2004). Cnot6/6L (Ccr4a/b) and Cnot7/8 (Caf1a/b), which belong to the exonuclease-endonuclease-phosphatase (EEP) family and the DEDD (Asp-Glu-Asp-Asp) family, respectively, possess deadenylase activity (Goldstrohm and Wickens, 2008). Subunits of the CCR4-NOT complex are ubiquitously expressed in adult mice with some tissue preferences, such as hematopoietic and metabolic tissue (Chen et al., 2011; Morita et al., 2011). Importantly, the deadenylase activities of the CCR4-NOT complex (Morita et al., 2011) and Nocturnin deadenylase (Green et al., 2007) are implicated in the control of obesity and energy metabolism. It appears that in liver, deadenylase activity is recruited to the 3′-end of mRNAs of energy metabolism-associated genes, shortening their lifespans and reducing their expression levels (Morita et al., 2011).

The Tob/BTG family of antiproliferative proteins is implicated in regulation of mRNA decay (Ezzeddine et al., 2012; Ogami et al., 2014). Tob binds to the CCR4-NOT complex through direct interaction with Cnot7 (Horiuchi et al., 2009). Upon translation termination, Tob competes with eukaryotic release factors (eRFs) and helps recruit CCR4-NOT deadenylases to the poly(A)

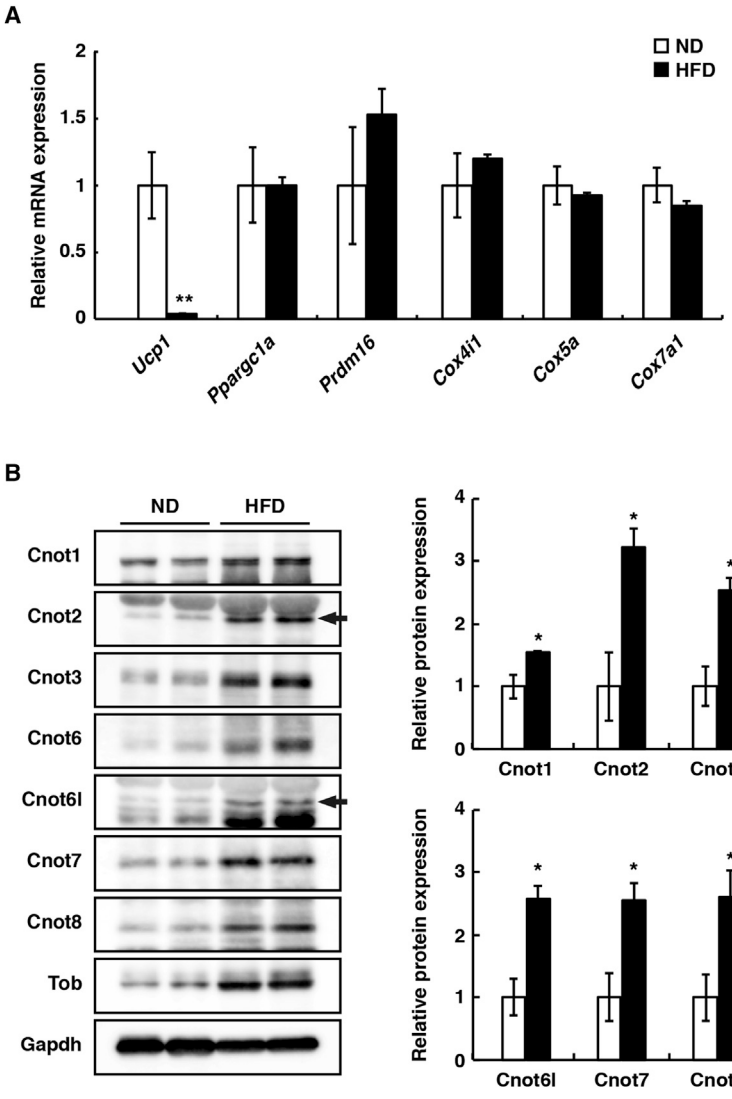

Figure 1. Expression Levels of Subunits of the CCR4-NOT Complex and Tob Are Negatively Correlated with Ucp1 Expression in Obese iWAT

(A) Real-time PCR analysis of *Ucp1*, *Ppargc1a*, *Prdm16*, *Cox4i1*, *Cox5a*, and *Cox7a1* mRNA levels in iWAT of mice on HFD and ND at 8 weeks of age for 12 weeks (n = 10; *p < 0.05). Mean ± SEM.

(B) Immunoblotting for Cnot1, Cnot2, Cnot3, Cnot6, Cnot6l, Cnot7, Cnot8, Tob, and Gapdh in iWAT of mice at 20 weeks of age after 12 weeks of HFD and ND feeding (left). The immunoblotting data are quantified and shown on the right (n = 3; *p < 0.05, **p < 0.01). Mean ± SEM.

tails of target mRNAs, such as c-*myc* mRNA, via interactions with poly(A)-binding protein (PABP) and cytoplasmic polyadenylation element-binding proteins (CPEBs) (Funakoshi et al., 2007; Ezzeddine et al., 2012; Ogami et al., 2014).

Here, we provide evidence that deficiency of *Cnot7* and *Tob* ameliorates diet-induced obesity. By addressing the roles of these proteins in energy metabolism, we found that stability of *Ucp1* mRNA is reduced by Tob-associated Cnot7 deadenylase, which suggests involvement of post-transcriptional mechanisms in *Ucp1* mRNA expression.

RESULTS

Upregulation of mRNA Decay Machinery Correlates with Suppression of *Ucp1* in iWAT of HFD-Induced Obese Mice

In iWAT of mice on a high-fat diet (HFD), Ucp1 expression is decreased, and thermogenesis is attenuated, driving promotion of obesity (Kopecký et al., 1995, 1996; Fromme and Klingenspor, 2011; Seale et al., 2011; Lee and Cowan, 2013). To explore the underlying mechanism of Ucp1 suppression, we assessed expression of genes encoding products that could alter thermogenesis in diet-induced obesity. Consistent with down-regulation of Ucp1, expression levels of *Ucp1* mRNA were dramatically decreased in iWAT of mice fed HFD, but not in mice fed a normal diet (ND), for a long term (12 weeks) (Figure 1A). In contrast, expression of other thermogenic genes (*Prdm16* and *Ppargc1a*) and electron transport chain-regulated genes (*Cox4i1*, *Cox5a*, and *Cox7a1*) was similar between ND and HFD mice (Figure 1A). Because expression of *Prdm16* and *Ppargc1a* was unchanged, we next examined expression of proteins that play a role in post-transcriptional regulation. We found that levels of Tob and subunits of the CCR4-NOT deadenylase complex, including Cnot1-3, Cnot6l, and Cnot6-8, were more than 1.5× higher in iWAT of HFD mice than in iWAT of ND mice (Figure 1B). The expression level of Cnot7 in BAT, mesenteric WAT, epididymal WAT (EpiWAT), and skeletal muscle was similar between ND and HFD mice (Figures S1A–S1D). In contrast to these observations on a long-term HFD feeding, short-term HFD feeding (4 weeks) resulted in increased expression of *Ucp1* mRNA as well as transcription factors, such as Prdm16 and Ppargc1a, which positively regulate *Ucp1* expression (Figure S1E). Upon short-term HFD feeding, the expression level of Tob, but not Cnot7, was also increased in iWAT (Figure S1F). After administration of a transcription inhibitor, actinomycin D, the remaining *Ucp1* mRNA level was lower in iWAT of HFD-fed mice than that in ND-fed mice (Figure S1G), suggesting that *Ucp1* mRNA destabilization was induced in iWAT from early stage of obesity. These results suggest that destabilization of *Ucp1* mRNA correlates with increase of Tob in iWAT from early stage of HFD-induced obesity. Increased levels of CCR4-NOT subunits also

contribute to suppression of *Ucp1* mRNA at least in late stage of obesity.

Resistance to Diet-Induced Obesity and Increment of Ucp1 Expression in the iWAT of HFD-Fed *Cnot7*$^{-/-}$ Mice

Cnot7$^{-/-}$ mice had significantly lower body weight than did WT mice that were fed a HFD for 12 or 24 weeks (Figures 2A and 2B). The suppressed weight gain in *Cnot7*$^{-/-}$ mice was not associated with food intake (Figure 2C). Weights of iWAT and visceral WAT were lower in *Cnot7*$^{-/-}$ than in WT mice (Figures 2D–2F), whereas weights of spleen, thymus, kidney, heart, lung, muscle, liver, and BAT showed no significant difference between WT and *Cnot7*$^{-/-}$ mice (Figure S2A). Histological analysis using H&E staining revealed that iWAT in HFD *Cnot7*$^{-/-}$ mice contained smaller adipocytes than in HFD WT mice (Figures 2G and 2H). Circulating blood glucose levels were significantly lower in fed and fasted *Cnot7*$^{-/-}$ mice compared with WT mice (Figure 2I). Insulin and glucose tolerance tests revealed that *Cnot7*$^{-/-}$ mice had enhanced insulin sensitivity and glucose clearance (Figures 2J and 2K). ND *Cnot7*$^{-/-}$ mice had smaller iWAT masses, though not significantly, than in WT, and body weights of *Cnot7*$^{-/-}$ mice were also slightly lower than those of WT mice (Figures S2B and S2C). Taken together, *Cnot7*$^{-/-}$ deficiency reduces diet-induced iWAT adiposity and obesity in mice.

To investigate the molecular mechanism underlying reduced iWAT mass in HFD *Cnot7*$^{-/-}$ mice, we performed quantitative RT-PCR analysis of genes that could regulate adipogenesis and adipocyte function. Intriguingly, we found that in the iWAT of HFD *Cnot7*$^{-/-}$ mice, *Ucp1* mRNA expression was greatly increased compared with HFD WT mice. The expression enhancement reflected the length of time on HFD (>3× after 12 weeks and >12× after 24 weeks) (Figures 3A and S3A). In contrast, expression of other thermogenic genes (*Prdm16*, *Ppargc1a*, and *Ucp2*), electron transport chain-regulated genes (*Cox4i1*, *Cox5a*, and *Cox7a1*), adipogenic genes (*Cebpa*, *Pparg1*, and *Pparg2*), and inflammatory genes (*Tnf* and *Ccl2*) was similar between *Cnot7*$^{-/-}$ and WT mice (Figures 3A). Consistent with upregulation of *Ucp1* mRNA, Ucp1 protein was also significantly more abundant in iWAT of *Cnot7*$^{-/-}$ mice (Figures 3B and 3C). In contrast, phosphorylation of hormone-sensitive lipase (HSL) at Ser660, which is relevant to lipolysis, and expression levels of Perilipin, which is a key regulator of lipid formation, were similar between HFD *Cnot7*$^{-/-}$ and WT mice (Figures 3B and 3C), suggesting that neither lipid catabolism nor anabolism was affected by the absence of Cnot7. Note that Ucp1-expressing adipocytes were increased in iWAT of *Cnot7*$^{-/-}$ mice compared with that in WT mice (Figure 3D). Ucp1 expression was significantly increased in EpiWAT and BAT of HFD *Cnot7*$^{-/-}$ mice compared with WT mice (Figures 3E and 3F), indicating that Cnot7 could inhibit Ucp1 expression in both white and BATs as well. Collectively, although Cnot7 deficiency does not affect lipolysis, adipogenesis, and inflammation, it remarkably increases *Ucp1* expression in iWAT of HFD mice. Moreover, energy expenditure was augmented in HFD *Cnot7*$^{-/-}$ mice, suggesting increased oxygen consumption (Figure 3G). Finally, Ucp1 expression was not significantly altered in ND *Cnot7*$^{-/-}$ mice compared with that in ND WT mice (Figure S3B).

Destabilization of *Ucp1* mRNA through Cnot7 Deadenylase Activity

We next examined the effect of Cnot7 on thermogenesis in adipocytes. Primary preadipocytes from iWAT of *Cnot7*$^{-/-}$ and WT mice were differentiated into mature adipocytes. Cnot7 did not affect adipogenesis per se because *Cnot7*$^{-/-}$ and WT cells underwent similar extent of differentiation, as shown by Oil-Red-O staining for lipid accumulation (Figure 4A). *Cnot7*$^{-/-}$ and WT adipocytes also expressed adipogenic genes at equivalent levels (*Cebpa*, *Pparg1*, and *Pparg2*) (Figure 4B). Among thermogenic genes, expression level of *Ucp1*, but not *Prdm16*, and *Ppargc1a*, was significantly increased in *Cnot7*$^{-/-}$ adipocytes compared with WT adipocytes (Figure 4B). Thus, *Cnot7* deficiency increases Ucp1 expression in an adipose cell-autonomous manner. Note that cellular oxygen consumption in adipocytes was not altered in the presence or absence of Cnot7 (Figure S4A).

We then addressed whether Cnot7 deadenylase activity is involved in regulation of *Ucp1* mRNA expression. *Ucp1* mRNA stability was assessed by actinomycin D-chase experiments using cultured preadipoctyes prepared from WT and *Cnot7*$^{-/-}$ mice. The half-life of *Ucp1* mRNA in *Cnot7*$^{-/-}$ cells (6.7 hr) was longer than in WT cells (4.2 hr) (Figure 4C). In contrast, half-lives of *Ppargc1a* and *Cox4i1* mRNAs were similar between *Cnot7*$^{-/-}$ and WT cells (Figure 4C). By examining the lengths of poly(A) tails, we found that *Ucp1* mRNA had a longer poly(A) tail in the absence of Cnot7 than in its presence (Figure 4D). Then, we subcloned the 3′-UTR of mouse *Ucp1* mRNA into the pGL3 luciferase vector. The reporter plasmid was introduced into HEK293 cells, which were subjected to actinomycin D-chase experiments in the presence of EGFP-fused human Cnot7 WT or Cnot7 H225A mutant, which lacks deadenylase activity (Horiuchi et al., 2009). The same quantities of EGFP-Cnot7 and EGFP-Cnot7 H225A proteins were expressed in HEK293 cells (Figure S4B). The half-life of luciferase-*Ucp1* 3′-UTR mRNA was longer in cells transfected with EGFP-Cnot7 H225A (14.7 hr) than in EGFP-Cnot7-introduced cells (7.3 hr) (Figure 4E). We further examined whether the CCR4-NOT complex interacts with *Ucp1* mRNA using an RNA immmunoprecipitation assay. Because *Ucp1* mRNA expression is very low in iWAT, we examined BAT lysates. In anti-Cnot3 immunoprecipitates, Cnot1, Cnot6l, and Cnot7 subunits of the CCR4-NOT complex were detected, indicating validity of the experimental system (Figure S4C). Importantly, *Ucp1* mRNA was found in anti-Cnot3 immunoprecipitates (Figure 4F). Therefore, we conclude that the Cnot7 deadenylase in the CCR4-NOT complex participates in destabilization of *Ucp1* mRNA.

As the CCR4-NOT complex is thought to be involved in degradation of multiple mRNA species dependent on context, we further scrutinized other candidate targets. We found that the expression level of the type 2 deiodinase (*Dio2*) mRNA was higher in iWAT of HFD *Cnot7*$^{-/-}$ mice compared with HFD WT mice (Figure S4D). Stability of *Dio2* mRNA was higher in *Cnot7*$^{-/-}$ cells than WT cells (Figure S4E). These results suggest that Cnot7 may also contribute to suppression of *Dio2* mRNA in obese iWAT. Interestingly, Dio2 converts thyroxin (T4) to 3,3′,5-triiodothyronine (T3) and is involved in thermogenesis (Christoffolete et al., 2004).

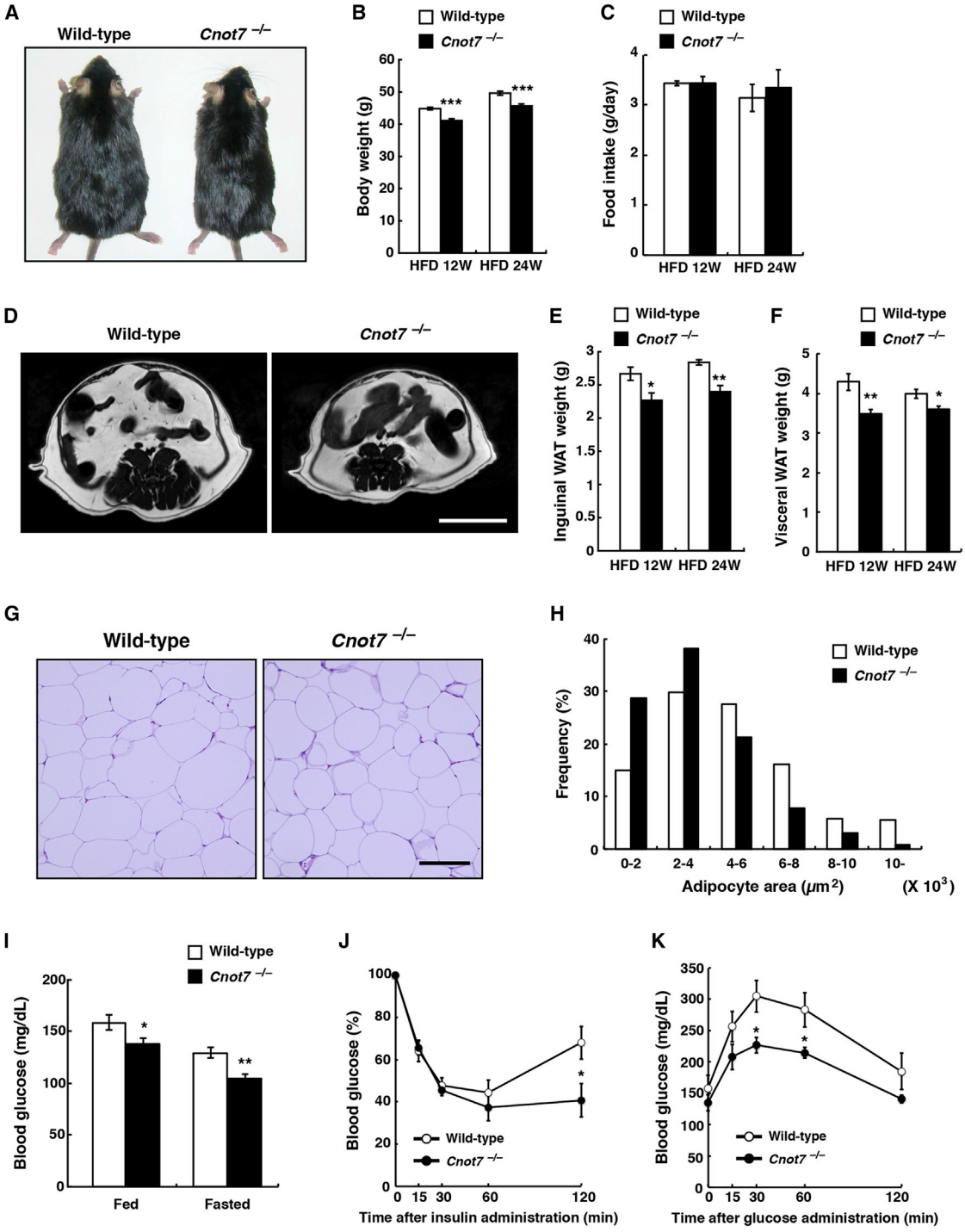

Figure 2. *Cnot7*$^{-/-}$ Mice on a HFD Show Decreased iWAT Mass and Resist Diet-Induced Obesity

Cnot7$^{-/-}$ and WT C57BL/6 mice were placed on a HFD at 8 weeks of age.

(A) Gross appearance of *Cnot7*$^{-/-}$ and WT mice-fed a HFD for 12 weeks.

(B) *Cnot7*$^{-/-}$ mice (n = 18 for 12 weeks, n = 6 for 24 weeks) showed decreased body weight compared with WT mice (n = 17 for 12 weeks, n = 6 for 24 weeks) (***p < 0.001). Mean ± SEM.

(C) Food intake did not differ between *Cnot7*$^{-/-}$ and WT mice-fed a HFD (n = 5 for 12 weeks, n = 4 for 24 weeks). Mean ± SEM.

(D) MRI evaluation of fat model in *Cnot7*$^{-/-}$ and WT mice fed a HFD for 12 weeks. Scale bar represents 1 cm.

(E and F) *Cnot7*$^{-/-}$ mice (n = 5 for 12 and 24 weeks) showed decreased iWAT (E) and visceral WAT (F) masses compared with WT mice (n = 8 for 12 weeks, n = 5 for 24 weeks) (*p < 0.05; **p < 0.01). Mean ± SEM.

(legend continued on next page)

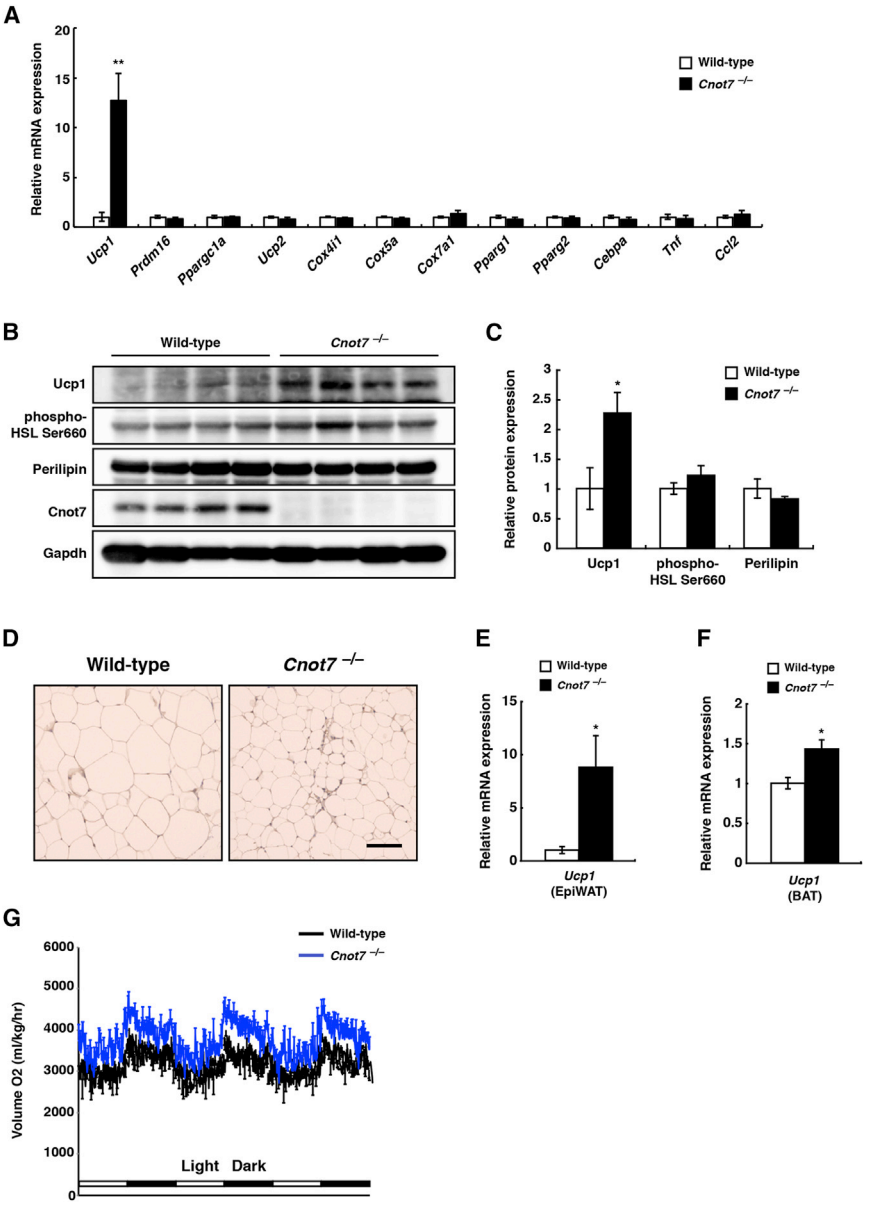

Figure 3. *Cnot7* Deficiency Increases Ucp1 Expression in Obese iWAT

Cnot7$^{-/-}$ and WT C57BL/6 mice were placed on a HFD at 8 weeks of age.

(A) Real-time PCR analysis of *Ucp1*, *Prdm16*, *Ppargc1a*, *Ucp2*, *Cox4i1*, *Cox5a*, *Cox7a1*, *Pparg1*, *Pparg2*, *Cebpa*, *Tnf*, and *Ccl2* mRNA levels in iWAT of WT and *Cnot7*$^{-/-}$ mice fed a HFD for 24 weeks (n = 4; **p < 0.01). Mean ± SEM.

(B and C) iWAT lysates of WT and *Cnot7*$^{-/-}$ mice-fed a HFD for 24 weeks were analyzed by immunoblotting with antibodies against Ucp1, phospho-HSL, Perilipin, Cnot7, and Gapdh (B). Quantification of the immunoblotting data is shown on the right (n = 4; *p < 0.05). Mean ± SEM (C).

(D) Immunohistochemistry for Ucp1 protein in iWAT of WT and *Cnot7*$^{-/-}$ mice on a HFD for 2 weeks. Scale bar represents 100 μm.

(E and F) Real-time PCR analysis of *Ucp1* mRNA levels in epididymal WAT (E) and BAT (F) of WT and *Cnot7*$^{-/-}$ mice fed a HFD for 24 weeks (n = 3; *p < 0.05). Mean ± SEM.

(G) Increased oxygen consumption in *Cnot7*$^{-/-}$ mice-fed a HFD for 12 weeks, compared with WT mice (n = 3). Mean ± SEM.

Facilitation of *Ucp1* mRNA Degradation by Tob

Tob directly interacts with the Cnot7 deadenylase subunit of the CCR4-NOT complex (Horiuchi et al., 2009) and is implicated in regulation of mRNA decay (Ezzeddine et al., 2012; Ogami et al., 2014). As expression of both Tob and Cnot7 in iWAT of HFD mice was inversely correlated with that of Ucp1 (Figures 1A and 1B), we hypothesized that Tob is also involved in regulation of *Ucp1* mRNA persistence. We first analyzed metabolic differences between HFD WT and *Tob*$^{-/-}$ mice and found that mice and their iWAT weighed less in the absence of Tob than in its presence (Figures 5A and 5B). BAT mass was also significantly lower in *Tob*$^{-/-}$ mice than in WT mice, whereas no significant difference was detected between *Tob*$^{-/-}$ and WT mice in spleen, kidney, heart, muscle, and liver (Figure S5A). Moreover, *Ucp1* mRNA expression levels were higher in iWAT of *Tob*$^{-/-}$ mice compared with WT mice (Figure 5C). Ucp1-expressing adipocytes were increased in iWAT of *Tob*$^{-/-}$ mice compared with WT mice (Figure 5D). These results suggest that Tob inhibits Ucp1 expression in iWAT.

To determine whether Tob is involved in regulation of *Ucp1* mRNA decay, we analyzed lengths of poly(A) tails and half-lives of *Ucp1* mRNA. Poly(A)-tails were apparently longer in iWAT of *Tob*$^{-/-}$ mice than in WT mice (Figure 5E). Stability of luciferase-*Ucp1* 3′-UTR reporter mRNA was lower in WT Tob expressing than W93ATob-expressing HEK293 cells (Figure 5F). Because Tob W93 is important for Tob-Cnot7 interaction

(G and H) H&E staining of iWAT in *Cnot7*$^{-/-}$ and WT mice fed a HFD for 24 weeks. Scale bar represents 100 μm (G). Distribution of adipocyte size in iWAT of *Cnot7*$^{-/-}$ and WT mice-fed a HFD for 24 weeks (H).

(I) *Cnot7*$^{-/-}$ mice had lower feeding (n = 4) and fasting (n = 5) circulating blood glucose than WT mice. Both groups received a HFD for 12 weeks.

(J) Insulin tolerance test (ITT). *Cnot7*$^{-/-}$ mice had lower blood glucose levels than WT mice (n = 4) after an intraperitoneal (i.p.) injection of 1.0 mU/g body weight of insulin (*p < 0.05). Both groups received a HFD for 4 weeks. Mean ± SEM.

(K) Glucose tolerance test (GTT). *Cnot7*$^{-/-}$ mice had lower blood glucose levels than WT mice (n = 5) after an i.p. injection of 0.5 mg/g body weight of glucose (*p < 0.05). Both groups were fed a HFD for 4 weeks. Mean ± SEM.

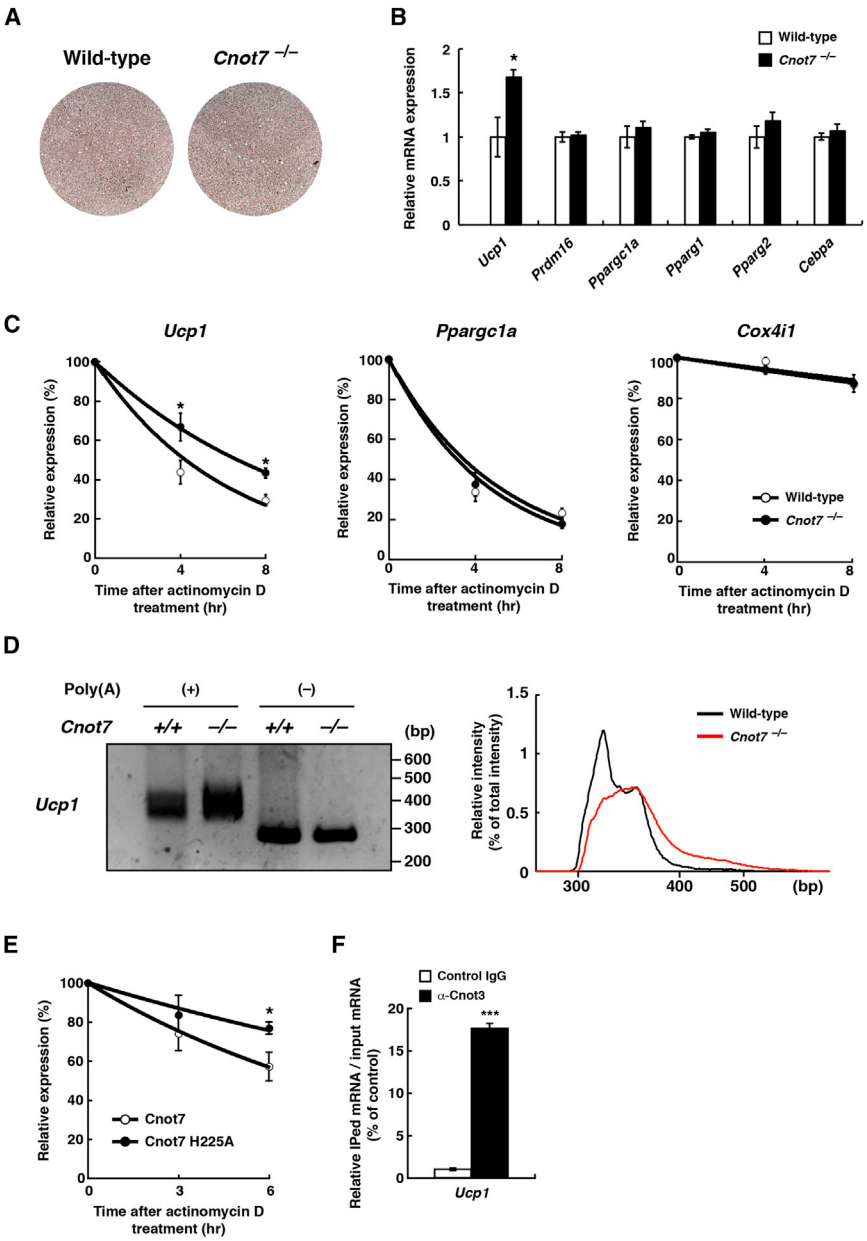

Figure 4. Cnot7 Destabilizes *Ucp1* mRNA

(A and B) Preadipocytes isolated from stromal vascular fraction of WT and *Cnot7*$^{-/-}$ mice were differentiated into adipocytes for 6 days. Oil-Red-O staining for lipid accumulation (A). Real-time PCR analysis of the *Ucp1*, *Prdm16*, *Ppargc1a*, *Pparg1*, *Pparg2*, and *Cebpa* mRNA levels in WT and *Cnot7*$^{-/-}$ adipocytes (n = 6; *p < 0.05) (B).

(C) Half-lives of *Ucp1*, *Ppargc1a*, and *Cox4i1* mRNA in WT and *Cnot7*$^{-/-}$ preadipocytes isolated from iWAT (n = 4; *p < 0.05). Mean ± SEM.

(D) *Cnot7*$^{-/-}$ mice were placed on a HFD for 24 weeks starting at 8 weeks of age. Poly(A) tail length of *Ucp1* mRNA in iWAT of *Cnot7*$^{-/-}$ and WT mice was analyzed by Poly(A) Tail-Length Assay Kit (left). Distribution of poly(A) tail length (right).

(E) HEK293 cells were transfected with pEGFP/Cnot7 or pEGFP/Cnot7 H225A for 24 hr and then transfected with luciferase-*Ucp1* 3′-UTR reporter for 12 hr. The half-life of luciferase-*Ucp1* 3′-UTR mRNA in Cnot7 WT and Cnot7 H225A-overexpressed HEK293 cells (n = 4; *p < 0.05). Mean ± SEM.

(F) BAT lysates were immunoprecipitated with mouse control IgG and anti-Cnot3 antibody. The levels of *Ucp1* mRNA in immune complex were analyzed by Real-time PCR (n = 3; ***p < 0.001). Mean ± SEM.

Note that *Cnot7* and *Tob* deficiencies did not affect expression levels of Tob and Cnot7, respectively (Figures S5C and S5D).

Role of BRF1 in Recruiting the CCR4-NOT Complex to the 3′-UTR of *Ucp1* mRNA for the Control of Its Stability

Since the 3′-UTR sequence of *Ucp1* mRNA contains AU-rich elements (AREs), including UAUUUAU (Figure 6A), we performed immunoprecipitation experiments using flag-tagged *Ucp1* 3′-UTR to search for RNA-binding proteins (RBPs) that interact with this element. We identified the TTP family of ARE-recognizing protein, BRF1, but not KSRP (another type of ARE-binding protein) nor TIA-1/TIAR, in immunoprecipitates (Figure 6B). To identify BRF1-interacting sequences in the *Ucp1* 3′-UTR, we performed a sequence-specific competition experiment using 12 bp of LNA (Locked Nucleic Acid)-oligonucleotides. The results indicated that BRF1 interacted with the *Ucp1* 3′-UTR through the UAUUUAU (oligo-2) sequence, but not UAUUUAC (oligo-1) nor UAUUUAA (oligo-3) sequence (Figure 6C). Other members of the TTP family of proteins, TTP and BRF2, also bound to the 3′-UTR of *Ucp1* mRNA through UAUUUAU sequence (Figures S6A–S6C). Additionally, BRF1 interacted with a 3′-UTR fragment of human *UCP1* mRNA, which includes a UAUUUAU sequence that localizes within the

(Figure 5G), the data suggest that Tob together with Cnot7 participates in deadenylation-induced *Ucp1* mRNA degradation. Furthermore, an RNA immunoprecipitation assay using lysates of luciferase-*Ucp1* 3′-UTR-expressing cells revealed that Tob interacted with luciferase-*Ucp1* 3′-UTR mRNA (Figure 5H) and with subunits of the CCR4-NOT complex, including Cnot1, Cnot6l, and Cnot9 (Figure S5B). Finally, flag-tagged *Ucp1* 3′-UTR sequences (Adachi et al., 2014) interacted, with low efficiency, with Cnot1 of the CCR4-NOT complex in HEK293 cells that overexpress Tob. The interaction barely occurred in those expressing a Tob W93A mutant (Figure 5I). The results suggest that Tob recruits Cnot7 of the CCR4-NOT complex to the 3′-UTR of *Ucp1* mRNA and facilitates its deadenylation.

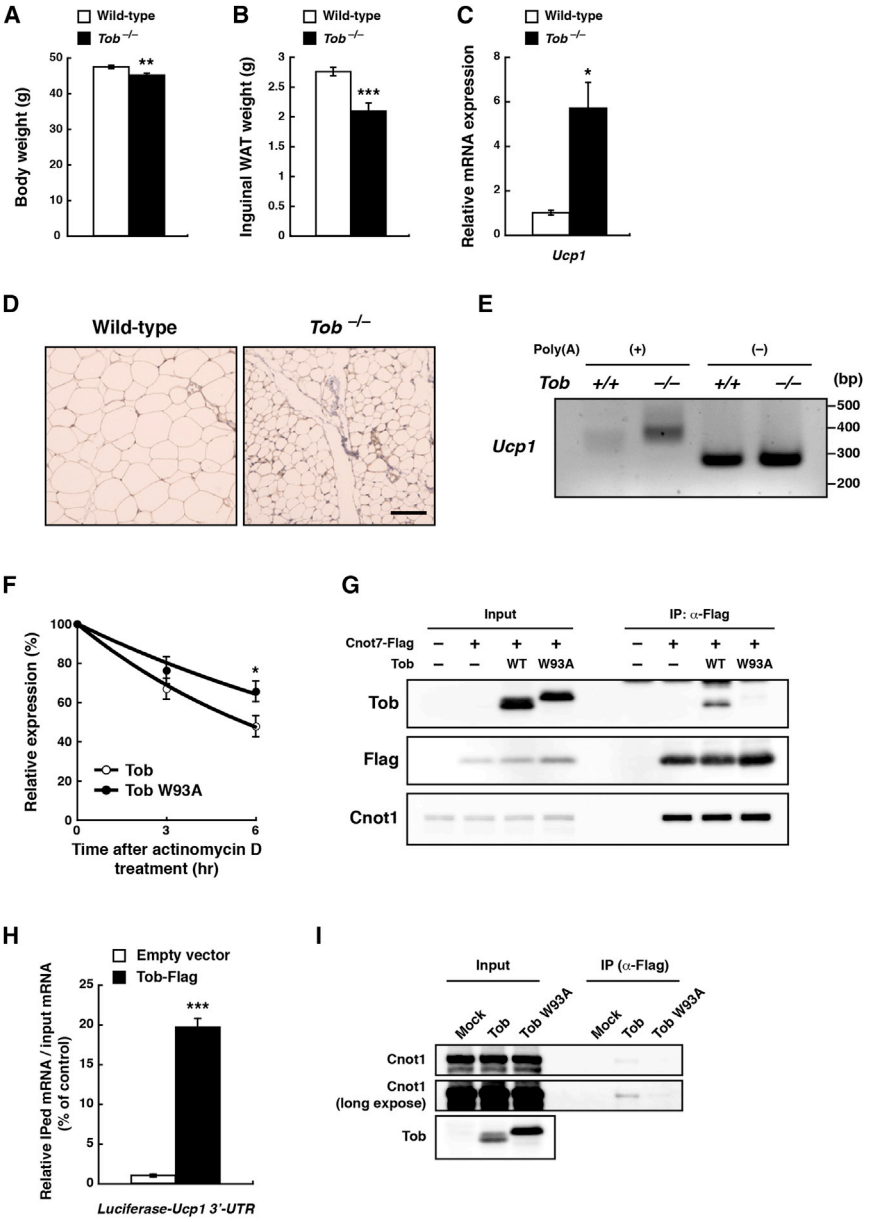

Figure 5. Tob Facilitates *Ucp1* mRNA Decay

(A and B) *Tob*$^{-/-}$ and WT C57BL/6 mice were placed on a HFD at 8 weeks of age for 12 weeks. *Tob*$^{-/-}$ mice had decreased body weight (n = 10) (A) and iWAT weight (n = 8) (B) compared with WT mice (**p < 0.01; ***p < 0.001). Mean ± SEM.

(C) Real-time PCR analysis of *Ucp1* mRNA levels in iWAT of *Tob*$^{-/-}$ and WT mice (n = 4; *p < 0.05). Mean ± SEM.

(D) Immunohistochemistry for Ucp1 protein in iWAT of WT and *Tob*$^{-/-}$ mice on a HFD for 2 weeks. Scale bar represents 100 μm.

(E) Poly(A) tail length of *Ucp1* mRNA in iWAT of *Tob*$^{-/-}$ and WT mice.

(F and G) HEK293 cells were transfected with pME18S/Tob or pME18S/Tob W93A for 24 hr and then transfected with luciferase-*Ucp1* 3′-UTR reporter for 12 hr. The half-life of luciferase-*Ucp1* 3′UTR mRNA was shorter in WT Tob than Tob W93A-overexpressed HEK293 cells (n = 6; *p < 0.05). Mean ± SEM (F). HEK293 cells were co-transfected with pME18S/Tob or pME18S/Tob W93A and pcDNA3/CNOT7-Flag vectors for 48 hr. The lysates of transfectants immunoprecipitated with anti-Flag antibody were analyzed by immunoblotting with antibodies against Tob, Flag, and Cnot1 (G).

(H) HEK293 cells were co-transfected with pcDEF empty or pcDEF/Tob-Flag and pGL3/*Ucp1* 3′-UTR vectors for 36 hr. By immunnoprecipitating with anti-Flag antibodies, enrichments of luciferase-*Ucp1* 3′-UTR mRNA in immune complexes were determined by real-time PCR (n = 3; ***p < 0.001). Mean ± SEM.

(I) HEK293 cells were transfected with pME18S/Tob, pME18S/Tob W93A for 36 hr. Cell lysates were incubated with Flag-tagged *Ucp1* 3′-UTR bait RNA for 1 hr and then immunoprecipitated with anti-Flag antibody. Immune complexes were analyzed by immunoblotting with antibodies against Cnot1 and Tob.

nucleotide sequence 345-414 (Figure S6D). Consistent with a previous report (Adachi et al., 2014), BRF1 interacted with the Cnot1 and Cnot7 subunits of the CCR4-NOT complex (Figure 6D). Co-immunoprecipitation experiments using lysates of flag-tagged Tob expressing cells showed that Tob interacted with BRF1 through both amino (N)- and carboxyl (C)-terminal regions (Figures 6E and S6E). Cnot1 of the CCR4-NOT complex was recruited to the *Ucp1* 3′-UTR by overexpression of BRF1 in HEK293 cells (Figure 6F). Moreover, stability of luciferase-*Ucp1* 3′-UTR reporter mRNA was higher in *BRF1* siRNA-treated HEK293 cells than in control cells (Figures 6G and S6F). Finally, to determine whether the BRF1-interacting ARE in *Ucp1* 3′-UTR affects its mRNA stability, we generated an ARE mutant of the *Ucp1* 3′-UTR reporter, in which the nucleotide sequence UAUUUAU was converted to UCUUUCU. BRF1 interaction with *Ucp1* 3′-UTR was attenuated by the mutation (Figure 6H), and the stability of luciferase-*Ucp1* 3′-UTR reporter mRNA with the mutated UCUUUCU sequence was higher than that with non-mutated sequence (Figure 6I). Taken together, these results suggest that BRF1, at least in part, reduces stability of *Ucp1* 3′-UTR through recruitment of Tob and Cnot7 in the CCR4-NOT complex to the ARE in the *Ucp1* 3′-UTR.

DISCUSSION

The CCR4-NOT deadenylase complex is involved in regulation of obesity. For example, deficiency of the *Cnot3* subunit in mice increases expression of genes related to ATP production in the liver (Morita et al., 2011). Here, we report that the Cnot7 deadenylase subunit of the CCR4-NOT complex is involved in control of obesity and adipose function. Increased expression of Cnot7 and its interacting partner Tob is observed in iWAT and

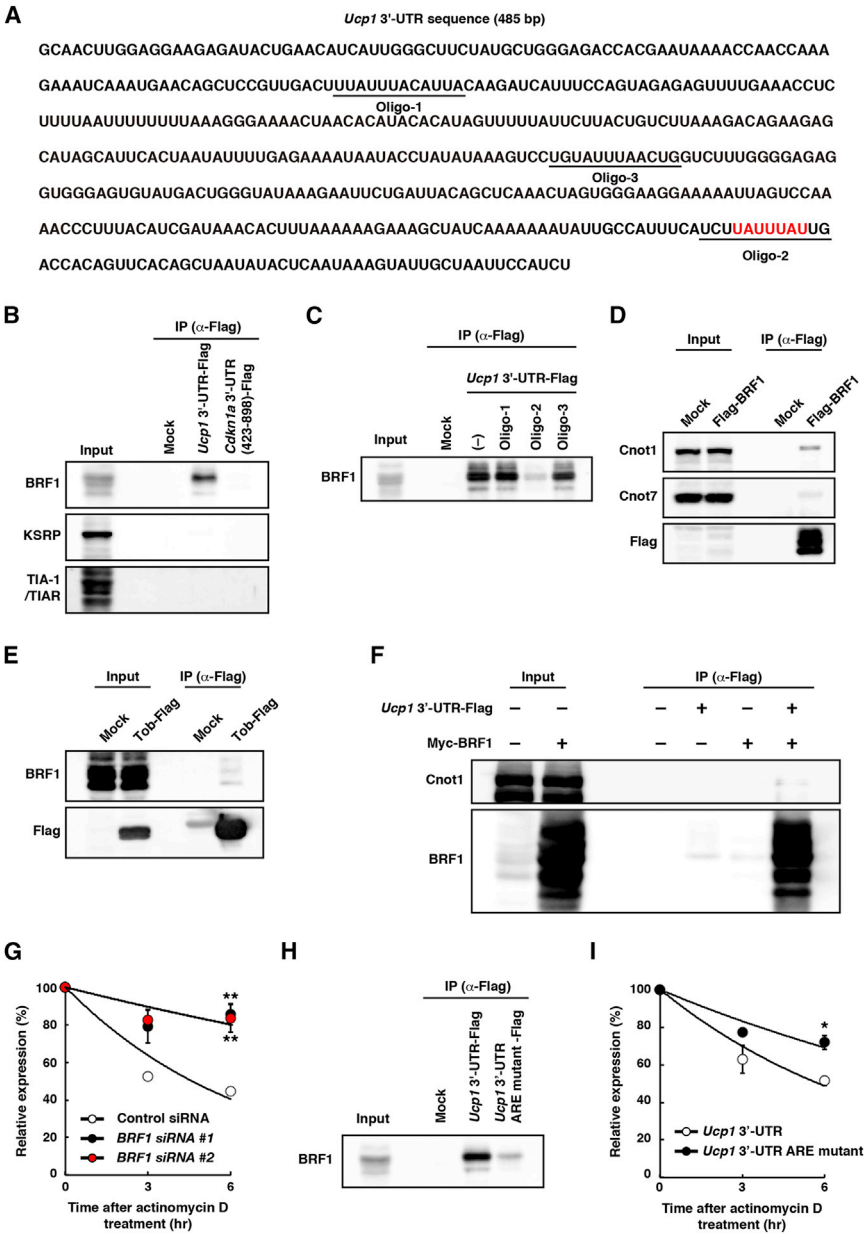

Figure 6. BRF1 Recruits the CCR4-NOT Complex to the 3′-UTR of *Ucp1* mRNA

(A) Sequence of the 3′-UTR of *Ucp1* mRNA (485 bp). The ARE (UAUUUAU) is colored red.

(B) Mouse liver lysates were incubated with Flag-tagged *Ucp1* and fragment of *Cdkn1a* 3′-UTR (nucleotide sequence at 423–898 from the first nucleotide of the *Cdkn1a* 3′-UTR) bait RNAs for 1 hr and then immunoprecipitated with anti-Flag antibody. Immune complexes were analyzed by immunoblotting with antibodies against BRF1, KSRP, and TIA-1/TIAR.

(C) Mouse liver lysates were incubated with Flag-tagged *Ucp1* 3′-UTR bait RNA in the presence or absence of 12 bp of complementary LNA-oligonucleotides for 1 hr. Immune complexes were analyzed by immunoblotting with antibodies against BRF1.

(D) HEK293 cells were transfected with Flag-tagged BRF1 for 36 hr. Cell lysates were immunoprecipitated with anti-Flag antibody. Immune complexes were analyzed by immunoblotting with antibodies against Cnot1, Cnot7, and Flag.

(E) HEK293 cells were transfected with pME18S/Tob-Flag or empty vectors for 36 hr. Cell lysates were immunoprecipitated with anti-Flag antibody. Immune complexes were analyzed by immunoblotting with antibodies against Flag and BRF1.

(F) HEK293 cells were transfected with Myc-tagged BRF1 for 36 hr. Cell lysates were incubated with Flag-tagged *Ucp1* 3′-UTR bait RNA for 1 hr and then immunoprecipitated with anti-Flag antibody. Immune complexes were analyzed by immunoblotting with antibodies against BRF1 and Cnot1.

(G) HEK293 cells were transfected with control, *BRF1* #1, and *BRF1* #2 siRNAs for 60 hr and then transfected with luciferase-*Ucp1* 3′-UTR reporter for 12 hr. The half-life of luciferase-*Ucp1* 3′-UTR mRNA in *BRF1* knockdown and control siRNA-treated HEK293 cells (n = 3; **p < 0.01). Mean ± SEM.

(H) Mouse liver lysates were incubated with Flag-tagged *Ucp1* 3′-UTR or *Ucp1* 3′-UTR with mutation in ARE for 1 hr and then immunoprecipitated with anti-Flag antibody. Immune complexes were analyzed by immunoblotting with antibodies against BRF1.

(I) HEK293 cells were transfected with luciferase-*Ucp1* 3′-UTR and *Ucp1* 3′-UTR with mutation in ARE for 12 hr. Half lives of mRNAs coding for luciferase-*Ucp1* 3′-UTR and *Ucp1* 3′-UTR with mutated ARE (n = 3; *p < 0.05). Mean ± SEM.

correlates with accumulation of fats in iWAT. Mice deficient in *Cnot7* and/or *Tob* store less fat than do WT mice. Accordingly, these mice are resistant to HFD-induced obesity and express remarkably increased levels of *Ucp1*. These observations are consistent with the observation that adipose tissue-specific *Ucp1* transgenic mice show resistance to diet-induced obesity and reduction of iWAT (Kopecký et al., 1995, 1996). Ucp1 expression also increases in cultured *Cnot7*$^{-/-}$ adipocytes, indicating that Cnot7 suppresses Ucp1 expression in an adipose cell-autonomous manner. Oxygen consumption is regulated by multiple factors and is unchanged in *Cnot7*$^{-/-}$ adipocytes in which Ucp1 increase is selective. In support, Ucp1 overexpression in 3T3-L1 adipocytes affects oxygen consumption minimally (Si et al., 2007). Thus, it appears that in iWAT of obese mice, Tob and Cnot7 inhibit Ucp1 expression.

Ucp1 is required in non-shivering thermogenesis, in which energy from the mitochondrial proton gradient is converted to heat, rather than to ATP (Rousset et al., 2004; Ricquier, 2011). Thermogenesis occurs in classic BAT and in brown adipocyte-like cells induced in iWAT at early stage of obesity or in response to cold acclimation (Madsen et al., 2010; Vitali et al., 2012). In contrast, expression of Ucp1 is reduced in iWAT of late stage obese mice (Fromme and Klingenspor, 2011; Lee and Cowan, 2013). Expression of *Ucp1* mRNA is controlled by transcription

factors, such as Pgc1α, Prdm16, Pparγ, and Zfp516 (Dempersmier et al., 2015; Puigserver et al., 1998; Seale et al., 2011). These factors bind to the promoter region of the *Ucp1* gene to control heat generation and body temperature (Harms and Seale, 2013; Wu et al., 2013). mRNA expression level is regulated by a balance between transcription and mRNA decay (Haimovich et al., 2013). At late stage of obesity, Cnot7 and Tob are induced in iWAT of HFD mice. As levels of transcription factors relevant to Ucp1 expression were not much affected, it appears that continuous nutrient enrichment selectively activates the Cnot7-Tob complex to deadenylate *Ucp1* mRNA, resulting in its degradation. At early stage of HFD-induced obesity, Pgc1α, Prdm16, and Tob, but not Cnot7, are increased, and *Ucp1* mRNA is destabilized in iWAT, suggesting simultaneous induction of transcription and mRNA decay. As mRNA decay fosters transcription (Haimovich et al., 2013), acute stimulation of *Ucp1* mRNA decay by Tob may facilitate *Ucp1* transcription during early stage of obesity. We also found that cold exposure decreases Cnot7 expression (A.T., unpublished data) and increases the level of the transcription factor, PGC1α, which upregulates *Ucp1* expression in iWAT (Fisher et al., 2012). Thus, apparently not only transcriptional induction, but also attenuation of deadenylation, contributes to increase Ucp1 to produce heat. Taken together, we propose the importance of *Ucp1* mRNA decay mediated by the Cnot7-Tob axis for fine regulation of thermogenic capacity in response to environmental factors.

BRF1 recognizes an AU-rich sequence at the 3′-UTR of *Ucp1* mRNA and is able to interact with Tob. As Cnot1 directly binds to TTP through a short C-terminal region that is conserved in BRF1 (Fabian et al., 2013), binding of BRF1 with N-terminal Tob, which interacts with Cnot7, may be via Cnot1. In addition, C-terminal Tob, which does not interact with Cnot7, binds to BRF1. Therefore, Cnot7 through its interaction with Tob and Cnot1 is recruited to BRF1-bound *Ucp1* mRNA for its deadenylation. In iWAT of age-matched HFD mice, compared with control, Ucp1 expression increases 3× and 6× with *Cnot7* and *Tob* deficiencies, respectively. As Tob interacts with Cnot7 via the lysine residue at 203 (Horiuchi et al., 2009) and it is conserved in Cnot8, Cnot8 may also be recruited by Tob, contributing to *Ucp1* mRNA degradation.

A similar role for Tob has been reported by Ogami et al. (2014). They showed that the Tob-Cnot7 axis mediates c-*myc* mRNA decay. They further showed that the polyadenylation element (CPE: UUUUUAU) on the 3′-UTR of c-*myc* mRNA is recognized by CPEB, which then recruits Cnot7 deadenylase to c-*myc* mRNA through an interaction with Tob, forming a ternary complex, CPEB-Tob-Cnot7. The complex negatively regulates expression of c-*myc* by accelerating deadenylation and decay of its mRNA. In quiescent cells, c-*myc* mRNA is destabilized by the CPEB-Tob-Cnot7 complex, while in serum-stimulated cells, c-*myc* mRNA is induced as an immediate early gene (Ogami et al., 2014). Thus, Tob is suggested to facilitate mRNA decay by recruiting Cnot7 deadenylase to poly(A) tails of target mRNAs. Interaction of Tob with sequence-specific RBPs may be important for target specificity of Cnot7 deadenylase.

MicroRNAs play an important role in deadenylation-induced mRNA decay and translation inhibition (Garneau et al., 2007; Goldstrohm and Wickens, 2008). *Ucp1* expression is increased by inhibition of *miR-106b*, and *miR-106b* is induced in BAT of HFD-fed mice (Wu et al., 2013). In addition, *miR-208b* is downregulated in BAT after cold exposure (Trajkovski et al., 2012). These reports suggest a negative correlation between *miR-106b* or *miR-208b* and Ucp1 expression. Moreover, Ago2 interacts with *Ucp1* 3′-UTR bait RNA (A.T., unpublished data), suggesting that the RISC complex is recruited to the 3′-UTR of *Ucp1* mRNA. Target Scan software analysis predicted that target sequences of *miR-208b* and *miR-106b* are present in the 3′-UTR region of *Ucp1* mRNA. These microRNAs may be incorporated into the RISC complex. To understand how Cnot7 targets *Ucp1* mRNA in iWAT upon HFD feeding, it will be necessary to determine whether certain miRNAs, such as *miR-208b* and *miR-106b*, are induced under these conditions, so that the RISC complex could function in tandem with BRF1-Tob-Cnot7 to deadenylate *Ucp1* mRNA.

It has been estimated that 5%–8% of human genes code for ARE-containing mRNAs (Barreau et al., 2005), raising the possibility that Cnot7-Tob-BRF1 axis regulates multiple transcripts that are involved in energy metabolism. Dio2 is involved in thermogenesis (Christoffolete et al., 2004), and we have found that *Dio2* mRNA increases in *Cnot7*$^{-/-}$ obese iWAT and is stabilized in *Cnot7*$^{-/-}$ cells. Moreover, a UAUUUAU sequence, which is a possible ARE for BRF1, is present in human and mouse 3′-UTR of *Dio2* mRNA. Thus, the Cnot7-Tob-BRF1 axis also contributes to silencing of *Dio2* mRNA to inhibit thermogenesis.

In conclusion, the Cnot7-Tob axis in the mRNA decay machinery post-transcriptionally downregulates *Ucp1* expression. Although the 3′-UTR sequences are not highly conserved in mouse and human *Ucp1* mRNA, interaction of BRF1 with human *UCP1* 3′UTR suggests that the Cnot7-Tob-BRF1 axis may suppress *UCP1* mRNA in human adipose tissue. Cnot7 and Tob may function as attenuators of adaptive thermogenesis under a high-calorie regimen, raising the possibility that Tob and Cnot7 could be useful therapeutic targets for obesity, because of their ability to destabilize *Ucp1* mRNA.

EXPERIMENTAL PROCEDURES

Mice

Cnot7$^{-/-}$ and *Tob*$^{-/-}$ mice have been described previously (Nakamura et al., 2004; Yoshida et al., 2000). We backcrossed *Cnot7*$^{-/-}$ and *Tob*$^{-/-}$ mice with C57BL/6J mice (from which *Cnot7*$^{-/-}$ and *Tob*$^{-/-}$ mice were derived) for at least eight generations. For all experiments, we maintained mice on a 12-hr light/12-hr dark cycle in a temperature-controlled (22°C) barrier facility with free access to water and either a normal diet (NCD, CA-1, CLEA Japan) or a HFD (HFD32, CLEA Japan). *Cnot7*$^{-/-}$, *Tob*$^{-/-}$, and WT mice were placed on HFD at 8 weeks of age for 4, 12, and 24 weeks. We used WT littermates as controls. For glucose tolerance tests, we deprived HFD mice of food for 16 hr and then injected them intraperitoneally with 0.5 mg glucose per g body weight. For insulin tolerance tests, we injected HFD mice intraperitoneally with 1.0 mU human insulin per g body weight. We collected blood samples and measured glucose concentrations with a glucometer (Glutest Pro, Sanwa Kagaku Kenkyusho). Oxygen consumption was measured with the Oxymax system (Columbus Instruments). Mouse experiments were approved by the animal experiment committees at The Institute of Medical Science, The University of Tokyo, and the Okinawa Institute of Science and Technology Graduate University.

MRI

Mice were scanned under isoflurane anesthesia using a 11.7 T Bruker MRI. For each mouse, the whole-body was imaged in accordance with an MRI protocol for fat tissues. Parameters for short T1-weighted spin-echo pulse sequences were repetition time = 360 ms, echo time = 20 ms, slice thickness = 1.0 mm, field-of-view = 3.5 × 3.5 (cm^2), matrix size = 320 × 320, average = 8. A fat image region was evaluated by visual inspection.

Histological Analysis of Tissue

After dissection, iWAT was fixed in 10% formaldehyde overnight and embedded in paraffin. Sections were stained with H&E. Immunohistochemistry for Ucp1 protein was performed with an antibody against Ucp1 (U6382; Sigma), according to the manufacturer's protocol.

Antibodies

Antibodies against the following were used: Cnot1, Cnot3, Cnot6, Cnot6l, Cnot7, and Cnot8 (mouse monoclonal antibodies; generated by Bio Matrix Research and Research Center for Advanced Science and Technology, The University of Tokyo), Cnot9 (rabbit polyclonal antibody; as described in Chen et al., 2011), Tob (mouse monoclonal and rabbit polyclonal antibodies), Cnot2 (#6955; Cell Signaling Technology), Ucp1 (ab10983; abcam; for western blotting), phospho-HSL (Ser660) (#4126; Cell Signaling Technology), Perilipin (#9349; Cell Signaling Technology), BRF1/2 (#2119; Cell Signaling Technology), KSRP (A302-021A; Bethyl Laboratories), TIA-1/TIAR (sc-28237; Santa Cruz Biotechnology), TTP (MABE65; Millipore), Flag (M2; Sigma), GFP (598; MBL), Myc (sc-40; Santa Cruz Biotechnology), and Gapdh (#2118; Cell Signaling Technology).

Plasmids

pDEST12.2/Myc- and Flag-BRF1 and BRF2 plasmids were kind gifts from Tohru Natsume (Adachi et al., 2014). Human Tob and Tob W93A were cloned into the pME18S vector (pME18S/Tob and pME18S/Tob W93A). Flag-tagged mouse Tob was cloned into the pME18S or pcDEF vectors (pcDEF/Tob-Flag and pME18S/Tob-Flag). Flag-tagged N-terminal Tob (1–113) and C-terminal Tob (114–345) were cloned into the pME18S vector (pME18S/Tob N-Flag and pME18S/Tob C-Flag). Flag-tagged full-length cDNA for human Cnot7 was cloned into the pcDNA3.1 (pcDNA3.1/Cnot7-Flag). EGFP-tagged human Cnot7 and Cnot7 H225A were cloned into pEGFP-C1 vectors (pEGFP/Cnot7 and pEGFP/Cnot7 H225A). Mouse *Ucp1* 3′-UTR (485 bp) was cloned into the pGL3 control vector (pGL3/*Ucp1* 3′-UTR). For generation of *Ucp1* 3′-UTR ARE mutant reporter, we substituted two adenines (A) into cytosines (C) (UUAUUUAUU (427-435) → UUCUUUCUU) in the BRF1-interacted ARE.

Cell Culture

HEK293T cells were cultured in DMEM containing 10% fetal bovine serum (FBS). For transient transfection, HEK293T cells were transfected using TransIT-LT1 (Takara) Transfection Reagent, according to the manufacturer's protocol. For half-life measurements of luciferase-*Ucp1* 3′-UTR mRNA, HEK293 cells were transfected with pEGFP/Cnot7, pEGFP/Cnot7 H225A, pME18S/Tob, or pME18S/TobW93A for 24 hr, or were transfected with human *BRF1* siRNAs (Catalog Number HSS101102 [*BRF1* #1], and HSS186138 [*BRF1* #2]; ThermoFisher Scientific) and control siRNA (as described in Takahashi et al., 2012a) for 60 hr and then transfected with the pGL3/*Ucp1* 3′-UTR vector for 12 hr. Cells were treated with 10 μg/ml actinomycin D (Wako) for 6 hr, and samples were collected at 0, 3, and 6 hr after treatment. For primary preadipocyte culture, preadipocytes were obtained from inguinal WAT of *Cnot7*$^{-/-}$ and WT mice. Adipose tissue was minced and digested in Hanks' balanced salt solution (HBSS; GIBCO) containing 1.5 U/ml Collagenase D (Roche) and 2.4 U/ml Dispase II (Roche) at 37°C for 45 min. Digestions were stopped with DMEM/F-12 containing 10% FBS. Cells were filtered through a 100-μm cell strainer (BD Falcon), centrifuged at 250 × *g* for 5 min, and cultured in DMEM/F-12 containing 10% FBS. For adipocyte differentiation, cells were stimulated with DMEM/F-12 containing 0.5 mM 3-isobutyl-1-methylxanthine (IBMX; Sigma), 1 μM dexamethasone (Sigma), 850 nM insulin (Sigma), 1 nM 3,3′,5-triiodo-L-thyronine (T3; Sigma), 125 μM indomethacin (Sigma), 1 μM rosiglitazone (Sigma), and 10% FBS for 2 days, and then the solution was replaced with DMEM/F-12 containing 850 nM insulin, 1 nM T3, 1 μM rosiglitazone, and 10% FBS every second day. Oil-Red-O staining method is described in a previous report (Takahashi et al., 2012b). Oxygen consumption was measured by Oxygen Consumption Rate Assay Kit (Cayman Chemical), according to the manufacturer's protocol. For the *Ucp1* mRNA half-life assay, preadipocytes were treated with 5 μg/ml actinomycin D for 8 hr, and samples were collected at time points of 0, 4, and 8 hr after treatment.

Quantitative Real-Time RT-PCR

Total RNA was isolated from iWAT and HEK293 cells using Isogen II (Nippongene), and cDNA was generated with SuperScript Reverse Transcriptase III (Invitrogen) as described previously (Takahashi et al., 2012a). cDNA was mixed with primers and SYBR Green Supermix (Takara) and analyzed with a Viia 7 sequence detection system (Applied Biosystems). Relative expression of mRNA was determined after normalization to mouse or human Gapdh levels using the ΔΔCt method. Primers are listed in Table S1.

Western Blotting

Western blotting was performed with enhanced chemiluminescence (Amersham Bioscience) as described previously (Takahashi et al., 2012b). iWATs were solubilized in TNE buffer (50 mM Tris-HCl [pH 7.5], 150 mM NaCl, 1 mM EDTA, 1% NP40, and 1 mM PMSF) for 30 min at 4°C. Lysates in SDS sample buffer were subjected to SDS-PAGE and electro-transferred onto polyvinylidene difluoride membranes. Protein bands were detected with appropriate antibodies and analyzed with ImageQuant software using an Image Analyzer LAS 4000 mini (GE Healthcare, Tokyo). Protein level was quantified using Image J software (NIH) and normalized by Gapdh level.

Poly(A) Tail Assay

Poly(A) tail length of *Ucp1* mRNA was measured using Poly(A) Tail-Length Assay Kit (Affymetrix) according to the manufacturer's protocol. For PCR, we used the following gene-specific primers: 5′-GCATAGCATTCACTAA TATTTTGAGAAAATAATACC-3′ for the forward primer and 5′-GGAATTAG CAATACTTTATTGAGTATATTAGCTG-3′ for the reverse primer. Poly(A) tail length was quantified with an Agilent High Sensitivity DNA Kit (Agilent Technologies) using an Agilent 2100 bioanalyzer (Agilent Technologies).

Protein and RNA Immunoprecipitations

For protein immunoprecipitation, HEK293 cells transfected with Flag-tagged proteins were solubilized in TNE buffer for 30 min at 4°C. Lysates were incubated with ANTI-FLAG M2 Affinity gel (Sigma) for 2 hr at 4°C. Proteins in immune complexes were immunoblotted with appropriate antibodies. For RNA immunoprecipitation, HEK293 cells were co-transfected with pGL3/*Ucp1* 3′-UTR and pcDEF/Tob-flag or pcDEF empty vectors for 36 hr using TransIT-LT1 Transfection Reagent. BAT was isolated from C57BL/6J WT mice at 9 weeks of age. Harvested cells and BAT solubilized in TNE buffer for 30 min at 4°C were incubated with antibodies against Flag and mouse control IgG (ab18413; abcam) or Cnot3, respectively, for 1 hr at 4°C, and then incubated with 50 μl of Dynabeads (Invitrogen) for 1 hr at 4°C. mRNAs in immune complexes were isolated using Isogen II, and cDNA was generated with SuperScript Reverse Transcriptase III. For quantitative real-time RT-PCR of the immunoprecipitated luciferase-*Ucp1* 3′-UTR mRNA, we used the following primer pairs that are designed in the 3′-UTR of *Ucp1* mRNA: 5′-ACTGGTCTTTGGGGAGAGGT-3′ for the forward primer and 5′-TCGATG TAAAGGGTTTTGGA-3′ for the reverse primer. For confirmation of protein immunoprecipitation with Dynabeads, proteins were immunoblotted with appropriate antibodies.

Preparation of Bait RNA and Analysis of RBPs

Flag-tagged mouse *Ucp1* 3′-UTR (485 bp) and fragment of *Cdkn1a* 3′-UTR (nucleotide sequence at 423–898 from the first nucleotide of the *Cdkn1a* 3′-UTR) bait RNA were generated as described previously (Adachi et al., 2014). For identification of *Ucp1* 3′-UTR binding proteins, livers from WT mice were solubilized in TNE buffer for 30 min at 4°C. Lysates were incubated with 10 pmol Flag-tagged *Ucp1* 3′-UTR bait RNA for 1 hr at 4°C and then incubated with ANTI-FLAG M2 Affinity gel for 1 hr at 4°C. For sequence-specific competition assay, all antisense-oligonucleotides against mouse *Ucp1* mRNA were fully LNA modified and were purchased from Gene

Design: Oligo-1 (5′-TAATGTAAATAA-3′), Oligo-2 (5′-TCAATAAATAAG-3′), and Oligo-3 (5′-CAGTTAAATACA-3′). Cytosines were methylated; 100 pmol oligonucleotides were incubated with 10 pmol Flag-tagged *Ucp1* 3′-UTR bait RNA. The bait RNA-protein complex was lysed in SDS-sample buffer, and bait RBPs were analyzed by immunoblotting.

Statistical Analyses

Comparisons were made using the unpaired Student's t test. Values represent the mean ± SEM and are represented as error bars. Statistical significance is as indicated.

SUPPLEMENTAL INFORMATION

Supplemental Information includes Supplemental Experimental Procedures, six figures, and one table and can be found with this article online at http://dx.doi.org/10.1016/j.celrep.2015.11.056.

AUTHOR CONTRIBUTIONS

A.T. performed most of the experiments with the assistance of M.M., M.T., and T.S. S.A. and T.N. provided essential materials. A.T. and T.Y. designed the study and wrote the manuscript.

ACKNOWLEDGMENTS

This work was supported by Grants-in-Aids for Scientific Research, 21229006; for Scientific Research in Innovative Areas, 25121734; and for Young Scientists, 25860761 from the Ministry of Education, Culture, Sports, Science, and Technology (MEXT), Japan. We thank the Okinawa Institute of Science and Technology Graduate University for generous support to T.Y.

Received: May 27, 2015
Revised: October 10, 2015
Accepted: November 17, 2015
Published: December 17, 2015

REFERENCES

Adachi, S., Homoto, M., Tanaka, R., Hioki, Y., Murakami, H., Suga, H., Matsumoto, M., Nakayama, K.I., Hatta, T., Iemura, S., and Natsume, T. (2014). ZFP36L1 and ZFP36L2 control LDLR mRNA stability via the ERK-RSK pathway. Nucleic Acids Res. *42*, 10037–10049.

Albert, T.K., Lemaire, M., van Berkum, N.L., Gentz, R., Collart, M.A., and Timmers, H.T. (2000). Isolation and characterization of human orthologs of yeast CCR4-NOT complex subunits. Nucleic Acids Res. *28*, 809–817.

Barreau, C., Paillard, L., and Osborne, H.B. (2005). AU-rich elements and associated factors: are there unifying principles? Nucleic Acids Res. *33*, 7138–7150.

Chen, C., Ito, K., Takahashi, A., Wang, G., Suzuki, T., Nakazawa, T., Yamamoto, T., and Yokoyama, K. (2011). Distinct expression patterns of the subunits of the CCR4-NOT deadenylase complex during neural development. Biochem. Biophys. Res. Commun. *411*, 360–364.

Christoffolete, M.A., Linardi, C.C., de Jesus, L., Ebina, K.N., Carvalho, S.D., Ribeiro, M.O., Rabelo, R., Curcio, C., Martins, L., Kimura, E.T., and Bianco, A.C. (2004). Mice with targeted disruption of the Dio2 gene have cold-induced overexpression of the uncoupling protein 1 gene but fail to increase brown adipose tissue lipogenesis and adaptive thermogenesis. Diabetes *53*, 577–584.

Collart, M.A., and Timmers, H.T. (2004). The eukaryotic Ccr4-not complex: a regulatory platform integrating mRNA metabolism with cellular signaling pathways? Prog. Nucleic Acid Res. Mol. Biol. *77*, 289–322.

Dempersmier, J., Sambeat, A., Gulyaeva, O., Paul, S.M., Hudak, C.S., Raposo, H.F., Kwan, H.Y., Kang, C., Wong, R.H., and Sul, H.S. (2015). Cold-inducible Zfp516 activates UCP1 transcription to promote browning of white fat and development of brown fat. Mol. Cell *57*, 235–246.

Ezzeddine, N., Chen, C.Y., and Shyu, A.B. (2012). Evidence providing new insights into TOB-promoted deadenylation and supporting a link between TOB's deadenylation-enhancing and antiproliferative activities. Mol. Cell. Biol. *32*, 1089–1098.

Fabian, M.R., Frank, F., Rouya, C., Siddiqui, N., Lai, W.S., Karetnikov, A., Blackshear, P.J., Nagar, B., and Sonenberg, N. (2013). Structural basis for the recruitment of the human CCR4-NOT deadenylase complex by tristetraprolin. Nat. Struct. Mol. Biol. *20*, 735–739.

Feldmann, H.M., Golozoubova, V., Cannon, B., and Nedergaard, J. (2009). UCP1 ablation induces obesity and abolishes diet-induced thermogenesis in mice exempt from thermal stress by living at thermoneutrality. Cell Metab. *9*, 203–209.

Fisher, F.M., Kleiner, S., Douris, N., Fox, E.C., Mepani, R.J., Verdeguer, F., Wu, J., Kharitonenkov, A., Flier, J.S., Maratos-Flier, E., and Spiegelman, B.M. (2012). FGF21 regulates PGC-1α and browning of white adipose tissues in adaptive thermogenesis. Genes Dev. *26*, 271–281.

Fromme, T., and Klingenspor, M. (2011). Uncoupling protein 1 expression and high-fat diets. Am. J. Physiol. Regul. Integr. Comp. Physiol. *300*, R1–R8.

Funakoshi, Y., Doi, Y., Hosoda, N., Uchida, N., Osawa, M., Shimada, I., Tsujimoto, M., Suzuki, T., Katada, T., and Hoshino, S. (2007). Mechanism of mRNA deadenylation: evidence for a molecular interplay between translation termination factor eRF3 and mRNA deadenylases. Genes Dev. *21*, 3135–3148.

Garneau, N.L., Wilusz, J., and Wilusz, C.J. (2007). The highways and byways of mRNA decay. Nat. Rev. Mol. Cell Biol. *8*, 113–126.

Goldstrohm, A.C., and Wickens, M. (2008). Multifunctional deadenylase complexes diversify mRNA control. Nat. Rev. Mol. Cell Biol. *9*, 337–344.

Green, C.B., Douris, N., Kojima, S., Strayer, C.A., Fogerty, J., Lourim, D., Keller, S.R., and Besharse, J.C. (2007). Loss of Nocturnin, a circadian deadenylase, confers resistance to hepatic steatosis and diet-induced obesity. Proc. Natl. Acad. Sci. USA *104*, 9888–9893.

Haimovich, G., Medina, D.A., Causse, S.Z., Garber, M., Millán-Zambrano, G., Barkai, O., Chávez, S., Pérez-Ortín, J.E., Darzacq, X., and Choder, M. (2013). Gene expression is circular: factors for mRNA degradation also foster mRNA synthesis. Cell *153*, 1000–1011.

Harms, M., and Seale, P. (2013). Brown and beige fat: development, function and therapeutic potential. Nat. Med. *19*, 1252–1263.

Horiuchi, M., Takeuchi, K., Noda, N., Muroya, N., Suzuki, T., Nakamura, T., Kawamura-Tsuzuku, J., Takahasi, K., Yamamoto, T., and Inagaki, F. (2009). Structural basis for the antiproliferative activity of the Tob-hCaf1 complex. J. Biol. Chem. *284*, 13244–13255.

Kopecký, J., Clarke, G., Enerbäck, S., Spiegelman, B., and Kozak, L.P. (1995). Expression of the mitochondrial uncoupling protein gene from the aP2 gene promoter prevents genetic obesity. J. Clin. Invest. *96*, 2914–2923.

Kopecký, J., Hodný, Z., Rossmeisl, M., Syrový, I., and Kozak, L.P. (1996). Reduction of dietary obesity in aP2-Ucp transgenic mice: physiology and adipose tissue distribution. Am. J. Physiol. *270*, E768–E775.

Lee, Y.K., and Cowan, C.A. (2013). White to brite adipocyte transition and back again. Nat. Cell Biol. *15*, 568–569.

Madsen, L., Pedersen, L.M., Lillefosse, H.H., Fjaere, E., Bronstad, I., Hao, Q., Petersen, R.K., Hallenborg, P., Ma, T., De Matteis, R., et al. (2010). UCP1 induction during recruitment of brown adipocytes in white adipose tissue is dependent on cyclooxygenase activity. PLoS ONE *5*, e11391.

Morita, M., Oike, Y., Nagashima, T., Kadomatsu, T., Tabata, M., Suzuki, T., Nakamura, T., Yoshida, N., Okada, M., and Yamamoto, T. (2011). Obesity resistance and increased hepatic expression of catabolism-related mRNAs in Cnot3+/− mice. EMBO J. *30*, 4678–4691.

Nakamura, T., Yao, R., Ogawa, T., Suzuki, T., Ito, C., Tsunekawa, N., Inoue, K., Ajima, R., Miyasaka, T., Yoshida, Y., et al. (2004). Oligo-astheno-teratozoospermia in mice lacking Cnot7, a regulator of retinoid X receptor beta. Nat. Genet. *36*, 528–533.

Ogami, K., Hosoda, N., Funakoshi, Y., and Hoshino, S. (2014). Antiproliferative protein Tob directly regulates c-myc proto-oncogene expression through

cytoplasmic polyadenylation element-binding protein CPEB. Oncogene *33*, 55–64.

Puigserver, P., Wu, Z., Park, C.W., Graves, R., Wright, M., and Spiegelman, B.M. (1998). A cold-inducible coactivator of nuclear receptors linked to adaptive thermogenesis. Cell *92*, 829–839.

Ricquier, D. (2011). Uncoupling protein 1 of brown adipocytes, the only uncoupler: a historical perspective. Front. Endocrinol. (Lausanne) *2*, 85.

Rousset, S., Alves-Guerra, M.C., Mozo, J., Miroux, B., Cassard-Doulcier, A.M., Bouillaud, F., and Ricquier, D. (2004). The biology of mitochondrial uncoupling proteins. Diabetes *53* (*Suppl 1*), S130–S135.

Seale, P., Conroe, H.M., Estall, J., Kajimura, S., Frontini, A., Ishibashi, J., Cohen, P., Cinti, S., and Spiegelman, B.M. (2011). Prdm16 determines the thermogenic program of subcutaneous white adipose tissue in mice. J. Clin. Invest. *121*, 96–105.

Si, Y., Palani, S., Jayaraman, A., and Lee, K. (2007). Effects of forced uncoupling protein 1 expression in 3T3-L1 cells on mitochondrial function and lipid metabolism. J. Lipid Res. *48*, 826–836.

Takahashi, A., Kikuguchi, C., Morita, M., Shimodaira, T., Tokai-Nishizumi, N., Yokoyama, K., Ohsugi, M., Suzuki, T., and Yamamoto, T. (2012a). Involvement of CNOT3 in mitotic progression through inhibition of MAD1 expression. Biochem. Biophys. Res. Commun. *419*, 268–273.

Takahashi, A., Morita, M., Yokoyama, K., Suzuki, T., and Yamamoto, T. (2012b). Tob2 inhibits peroxisome proliferator-activated receptor γ2 expression by sequestering Smads and C/EBPα during adipocyte differentiation. Mol. Cell. Biol. *32*, 5067–5077.

Trajkovski, M., Ahmed, K., Esau, C.C., and Stoffel, M. (2012). MyomiR-133 regulates brown fat differentiation through Prdm16. Nat. Cell Biol. *14*, 1330–1335.

Vitali, A., Murano, I., Zingaretti, M.C., Frontini, A., Ricquier, D., and Cinti, S. (2012). The adipose organ of obesity-prone C57BL/6J mice is composed of mixed white and brown adipocytes. J. Lipid Res. *53*, 619–629.

Wu, J., Cohen, P., and Spiegelman, B.M. (2013). Adaptive thermogenesis in adipocytes: is beige the new brown? Genes Dev. *27*, 234–250.

Yoshida, Y., Tanaka, S., Umemori, H., Minowa, O., Usui, M., Ikematsu, N., Hosoda, E., Imamura, T., Kuno, J., Yamashita, T., et al. (2000). Negative regulation of BMP/Smad signaling by Tob in osteoblasts. Cell *103*, 1085–1097.